Nanoscale

PAPER

View Article Online
View Journal | View Issue



Cite this: *Nanoscale*, 2022, **14**, 12265

# Solution and interfacial self-assembly of *Bacillus subtilis* bacterial lipoteichoic acid (LTA): nanoclustering, and effects of $Ca^{2+}$ and temperature†

Bhavesh Bharatiya,[a] Magdalena Wlodek,[b] Robert Harniman,[a] Ralf Schweins,[c] Judith Mantell,[d] Gang Wang,[a] Piotr Warszynski[b] and Wuge H. Briscoe *[a]

Lipoteichoic acid (LTA) is a major structural and functional molecule in the Gram-positive bacteria membrane. Knowledge of LTA adsorption at interfaces and its solution self-assembly is crucial to understanding its role in bacterial adhesion and colonisation, infections and inflammations. Here, we report the self-assembly behaviour of LTA extracted from *Bacillus subtilis*, a Gram-positive bacterium, in an aqueous solution using cryogenic transmission electron microscopy (Cryo-TEM) and small-angle neutron scattering (SANS) and its adsorption behaviour at the solid–liquid interface using atomic force microscopy (AFM) imaging and quartz crystal microbalance with dissipation monitoring (QCM-D). The Cryo-TEM results indicated the formation of spherical LTA micelles that decreased in size on addition of calcium chloride ($CaCl_2$), attributed to charge neutralisation and possible formation of stable $Ca^{2+}$-bridges between the phosphate groups on neighbouring LTA chains. Analysis of the SANS data from the polydisperse LTA aggregates in solution using the *two Lorentzian model* revealed the existence of two correlation lengths, which could respectively account for the presence of LTA micelle clusters and the local structure arising from LTA intra-molecular interactions. In the presence of $CaCl_2$, the decrease in the correlation lengths of the clusters indicated possible disruption of H-bonding by $Ca^{2+}$, leading to poorer water-LTA interactions. At higher temperatures, the correlation length corresponding to the clusters increased, indicating a temperature assisted growth caused by the fluidization of micellar core and dehydration of the polar LTA chains. AFM imaging showed that adsorption of LTA aggregates at the $SiO_2$–water interface was significantly prompted by the addition of $CaCl_2$, also confirmed by QCM-D measurements. These unprecedented nanoscopic structural details on the morphology of LTA aggregates in solution and at the solid–liquid interface add to our fundamental understanding of its self-assembly behaviour hitherto underexplored.

Received 31st January 2022,
Accepted 15th July 2022

DOI: 10.1039/d2nr00595f

rsc.li/nanoscale



## Introduction

Lipoteichoic acid (LTA) is an important biopolymer present in the Gram-positive bacteria membrane, playing both structural and functional roles. LTA is anchored to the phospholipid membrane through its diacylglycerol and its glycerophosphate chain expands over the extracellular peptidoglycan layer (Fig. 1A). The glycerophosphate chain comprises ~25–30 phosphodiester-linked repeating units (Fig. 1B), which may also contain ~5–10 mol% glycosyl or D-alanyl ester units depending on bacterial growth conditions.[1] The interfacial interactions leading to bacterial adhesion and colonisation are reportedly influenced by bacterial surface proteins and LTAs that expand towards the cell exterior.[2–4] LTA is considered as a major virulence factor for various infections and inflammations caused by Gram positive bacteria. It is released from bacterial cells after the bacteriolysis and upon interactions with cationic peptides or β-lactam antibiotics. LTA can attach to target cells though CD14 and toll-like receptors, whilst non-specific binding with the membrane phospholipids also occurs. The fundamental understanding of self-assembled LTA structures is essential, considering its amphiphilic character, which may influence several biological functions.[1]

[a]*School of Chemistry, University of Bristol, Cantock's Close, Bristol BS8 1TS, UK. E-mail: wuge.briscoe@bristol.ac.uk; Tel: +44 (0)117 3318256*
[b]*Jerzy Haber Institute of Catalysis and Surface Chemistry, Polish Academy of Sciences, Niezapominajek 8, PL-30239 Krakow, Poland*
[c]*Institut Laue-Langevin, DS/LSS, 71 Avenue des Martyrs, Grenoble 38000, France*
[d]*Wolfson Bioimaging Facility, University of Bristol, Medical Sciences Building, University Walk, Bristol BS8 1TD, UK*
† Electronic supplementary information (ESI) available. See DOI: https://doi.org/10.1039/d2nr00595f

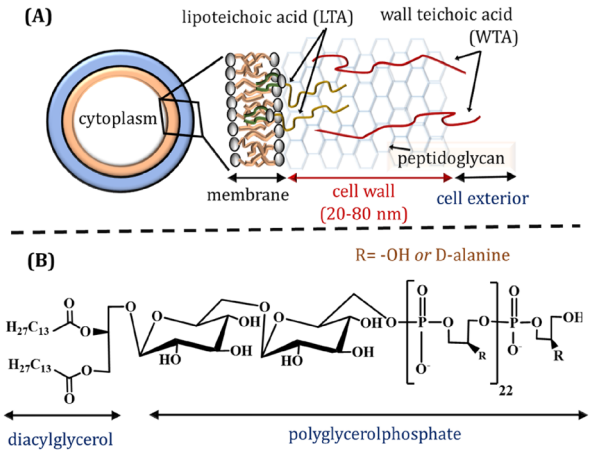


Fig. 1 (A) Schematic representation of Gram-positive bacteria cell wall. (B) Structure *of Bacillus subtilis* lipoteichoic acid (LTA).

The molecular self-assembly behaviour of LTA both in the solution and at the interfaces, such as the aggregate morphology and its response to solution conditions, is not well understood, despite the importance of such fundamental knowledge to the LTA role in infectivity, inflammation, and septic shock. It has been previously reported that surface active LTA molecules self-assemble to form aggregates in aqueous solutions driven by their amphiphilic properties. Wicken *et al.*[5] measured the critical micelle concentration (CMC) of LTA extracted from *Lactobacillus fermentum* by fluorescence spectroscopy using merocyanine dye as a probe, obtaining CMC values of 1–10 μg $mL^{-1}$ (~$0.2 \times 10^{-6}$ M to $2 \times 10^{-6}$ M). Courtney *et al.*[6] calculated the CMC of LTA extracted from different cocci in phosphate buffered saline (PBS) solutions as 28–60 μg $mL^{-1}$ (~$5.6 \times 10^{-6}$ M to $12.1 \times 10^{-6}$ M). These values are considerably higher than the CMC of ~$10^{-10}$ M observed for membrane phospholipids, which is due to the presence of the bulky hydrophilic glycerophosphate chain in the LTA structure, increasing its partitioning in aqueous bulk solutions.[7,8]

Several findings have implicated the function of monomeric LTA at low concentrations of ~0.3 to 2 μg $mL^{-1}$ – below its reported CMC – in various biological processes, *e.g.* maximum sensitisation of erythrocytes[9] and stimulation of lysosomal enzymes from the macrophages.[10] On the other hand, *Streptococcus pyogenes* LTA at concentrations higher than its CMC has been reported to induce disruption of erythrocytes in sheep and cause cytotoxicity to Girardi heart cells.[6] These reports suggest significantly different responses to various biological processes by LTA molecules in both monomeric and aggregated states.

Labischinski *et al.*[11] investigated micellar structures formed by LTA extracted from *Bifidobacterium bifidum* DSM 20239, *Enterococcus hirae* (*Streptococcus faecium*) ATCC 9790, *Lactococcus garviue* NCDO 2155, *Listrria welshimeri* SLCC 5354, and *Staphylococcus aureus* DSM 20233. Their small angle X-ray scattering (SAXS) analysis revealed spherical micelles with the core formed by the lipophilic chains in an α-type conformation and the shell formed by the hydrophilic glycerophosphate chains. Approximately 150 LTA molecules aggregated to form a micelle with an average diameter of ~23 nm and a hydrophilic shell ~8.5 nm in thickness. The chains were assumed to aggregate in a coiled conformation to satisfy steric requirements and rationalise the obtained micelle size. Fischer *et al.*[12] determined the aggregation parameters for LTA extracted from *Streptococcus pneumoniae* using SAXS, reporting the formation of micelles with identical dimensions as observed by Labischinski *et al.*[11] The hydrophilic chains were assumed to adopt a fully extended conformation based on the calculations from the structural dimension of the micelle and the LTA molecule. These findings indicate that the supramolecular structure of LTA is controlled mainly by the cross-sectional area of lipophilic diacylglycerol moieties and presumably less influenced by the hydrophilic chain structure. On the other hand, our recent report[13] showed that the large molecular footprint and electrostatic characteristics of LTA also influenced the stability and integrity of the model phospholipid membrane. We found that mixed vesicles comprising *Bacillus subtilis* LTA and phospholipids showed an increase in the size as more LTA was added up to 6.5 mol%, while further LTA addition resulted in the partition of LTA from the mixed liposomes, leading to the coexistence of nascent LTA micelles and mixed LTA-lipid vesicles.

Understanding intermolecular interactions and self-assembled structures of bacterial lipids at various interfaces as well as in solution is of fundamental relevance to advancing our knowledge of bacterial functions.[1,14,15] To the best of our knowledge, the self-assembly behaviour of LTA extracted form *Bacillus subtilis* has not been reported previously. In this study, we have investigated the aggregation of LTA in aqueous solution and their adsorption at the solid–liquid interface using cryogenic transmission electron microscopy (Cryo-TEM), small angle neutron scattering (SANS), atomic force microscopy (AFM) imaging, and quartz crystal microbalance with dissipation monitoring (QCM-D). The effects of the addition of $Ca^{2+}$ at different concentrations and the solution temperature have also been investigated. We note that these observations were made in a model system, whereas the real biological system is much more complex. The nanoscopic morphological and structural information on LTA aggregates obtained using quantitative physical methods in the model system, however, is valuable to understanding the functional role of LTA in complex biological processes.

## Materials and methods

The lipoteichoic acid (LTA) extracted from *Bacillus subtilis* and $CaCl_2$ were purchased from Sigma-Aldrich, UK. Ultrapure water (resistivity 18.2 MΩ cm and total organic content (ToC) < 4 ppb) used for sample preparation was purified using Millipore® water purification system. Samples for SANS have been prepared in $D_2O$ instead of $H_2O$.

### Cryogenic-transmission electron microscopy (Cryo-TEM)

Cryo-TEM samples were prepared by plunge freezing performed using a LEICA GP, into liquid $N_2$-cooled liquid ethane. Droplets (~4–8 μL) of LTA in pure and mixed solutions with $CaCl_2$ were placed on glow discharged lacey carbon grids and left for 2 s before blotting (2 s) and plunging. This yielded samples with LTA aggregates embedded in the vitreous ice suspended inside the holes of the carbon grid. The sample grid was then transferred into a Gatan 626 cryo-holder and visualized at 200 kV in a Tecnai T20, FEI transmission electron microscope fitted with an FEI CETA camera. The images were analyzed using FIJI ImageJ® programme to generate the size histogram. All the images were taken using the same operational parameters to allow direct comparison of the structural changes.

### Quartz crystal microbalance with dissipation monitoring (QCM-D)

The deposition of 0.2 mg $mL^{-1}$ LTA in ultrapure Milli-Q water and in 10 mM aqueous $CaCl_2$ solution was studied *in situ* using the QCM-D (Q-Sense AB Gothenburg, Sweden; present name: Biolin Scientific). The QCM-D technique provides real-time information about the mass and structural properties of adsorbed species. It is based on measuring the resonant frequency of a disk-shaped piezoelectric quartz crystal with metal electrodes deposited on both sides. For a rigid film on the crystal, a small mass of adsorbate added to the electrodes induces a decrease in the resonant frequency ($\Delta f$), which is proportional to the mass deposited ($\Delta m$), according to Sauerbrey's relationship:[16–18]

$$\Delta m = -C\frac{\Delta f}{N} \quad (1)$$

where $C$ is a constant that depends on the physical properties of the quartz crystal (in our system $C$ = 17.7 ng $cm^{-2}$ $Hz^{-1}$) and $N$ is the crystal oscillation overtone number (*i.e.* $N$ = 1, 3, 5, 7, ...). The Sauerbrey relationship can be used only when the difference between the dissipation values for the measured overtones does not exceed $10^{-6}$, otherwise the Voigt viscoelastic model of the adsorbed film should be applied.[19]

The $SiO_2$-coated 5 MHz QCM-D crystals were purchased from Q-Sense AB (Sweden) and cleaned with piranha solution (a mixture of equivalent volumes of concentrated sulfuric acid and hydrogen peroxide) before the first use. After being dipped into the piranha solution for 2 min, the crystal substrates were then rinsed thoroughly with Milli-Q water, followed by 30 min immersion in hot (*ca.* 70 °C) Milli-Q water before dried in a stream of pure nitrogen prior to measurements. The crystals were mounted in the flow chamber of the instrument. After resonance frequency calibration, the chamber was filled with Milli-Q water to obtain a baseline. Then, the LTA dispersion was introduced, and the adsorption kinetics was monitored *in situ*. After obtaining a constant value of the resonance frequency, the chamber was rinsed. The Sauerbrey and Voigt viscoelastic model, implemented in QTools 3 software (Q-Sense AB)[16,18] was used to analyse the experimental data of LTA in ultrapure Milli-Q water and in 10 mM aqueous $CaCl_2$ solution, respectively. All the measurements were performed at 25 °C.

### Atomic force microscopy (AFM)

AFM (Bruker Multimode 8, Peakforce feedback control) was used to image the morphology of LTA aggregates absorbed on $SiO_2$ wafers. The ~1 cm × 1 cm $SiO_2$ substrate pieces were cleaned by rinsing with ethanol, dried with a nitrogen flow and UV-ozoned (UVO CLEANER®, Jelight Company Inc., US) for 20 min. It was then glued onto an AFM magnetic stub using Epon 1004 (Shell), and the substrate was incubated overnight in ~30 mL of sonicated 2 mg $mL^{-1}$ LTA aqueous dispersion (either in Milli-Q water or 10 mM $CaCl_2$ solution) at 25 or 40 °C. The stub was then transferred to the AFM with a drop of the solution deposited atop to ensure the surface was not dried and exposed to air. A liquid cell containing water or $CaCl_2$ solution was then mounted above the surface to keep it submerged throughout the measurement. PeakForce atomic force microscopy was conducted utilising a Multi-mode VIII microscope with Nanoscope V controller. SCANASYST-FLUID+ cantilevers (Bruker, CA, US) were used with a nominal tip radius and spring constant of 2 nm and 0.7 N $m^{-1}$, respectively. The Peakforce amplitude and setpoint were 50 nm and 0.8–1 nN, respectively. Images were obtained in tapping mode, at 512 × 512 pixels at a scan rate of 0.5 Hz except for 250 nm × 250 nm scans which were collected at 256 × 256 pixels at a scan rate of 1 Hz. Images were recorded and processed, including flattening to account for sample tilting and low pass filters to smoothen the image, using the Bruker NanoScope Analysis 1.80 software package.

### Small angle neutron scattering (SANS) measurements

SANS data was obtained from 2 mg $mL^{-1}$ LTA samples contained in quartz cells with a 2 mm path length on the D11[20–22] small-angle diffractometer at the Institut Laue-Langevin, ILL, (Grenoble, France). A neutron beam with wavelength ($\lambda$ = 5.5 Å with a FWHM of 9%) and sample-to-detector distance distances of 39 m, 8 m and 1.4 m were used to obtain a $q$-range of ~0.0016–0.5 $Å^{-1}$, where $q = 4\pi \sin(2\theta/2)/\lambda$ is the momentum transfer with $2\theta$ the scattering angle. The neutron beam used had a size of 7 × 10 $mm^2$. A $^3$He MWPC detector with 256 × 256 pixels of 3.75 × 3.75 $mm^2$ each was used to record the scattered intensities. The raw scattering data were corrected for the detector efficiency, sample transmission, and background scattering and converted to scattering cross-section data ($\partial\Sigma/\partial\Omega$ *vs.* $q$) using LAMP software. The data was converted to an absolute scale ($cm^{-1}$) using the secondary calibration standard $H_2O$ of 1 mm path length (cross-calibrated against an h/d polymer blends sample) with a differential scattering cross-section of 0.956 $cm^{-1}$.

### Analysis of SANS data

The SANS data were analysed using the two-Lorentzian model[23] with the following equation,

$$I(q) = \frac{A}{1+(Q\xi_1)^n} + \frac{C}{1+(Q\xi_2)^m} + B \quad (2)$$

where $I(q)$ is the scattering intensity, $q$ the scattering vector, $A$ the Lorentzian scale factor 1, $C$ the Lorentzian scale factor 2, $\xi_1$ and $\xi_2$ the respective correlation lengths, and $n$ and $m$ the

respective power-law components. This model calculates an empirical functional form for the SANS data characterised by two Lorentzian-type functions. The first term (with a subscript 1) describes the low-$q$ structures, while the second term (with a subscript 2) the high-$q$ structures. A background constant B ($q$-independent) has been introduced to account for the incoherent scattering at high-$q$. The correlation length values give an indication of the variation in the length scales with the concentration or density fluctuations in the system. The exponent $n$ characterises the fractal structure of the long-range inhomogeneities in the low-$q$ range. Here, $n > 3$ indicates a decrease in the solubility of scatterers and intra-molecular interactions being favoured. The exponent $m$ (high-$q$) informs on the extent of water–biopolymer interactions and hence the chain thermodynamics. We have trialled fitting the SANS data with shape-dependent models, such as sphere, core–shell sphere, core–shell ellipsoid, and triaxial ellipsoid models (*cf.* Fig. S1(b–e) in ESI†). However, due to the polydisperse nature of the aggregates, the fitting was not satisfactory. In the main text of this ms, we have focused on discussing the two Lorentzian model as it allowed fitting of the SANS data in both low-$q$ and high-$q$ regimes simultaneously. Furthermore, we have also trialled fitting the SANS data in different $q$ ranges using different models (*cf.* Fig. S1(b–e) in ESI†). The low-$q$ data could be well described by the fractal model, whilst the high-$q$ data by the correlation length model, as discussed in ESI.†

## Results and discussion

First, we would like to comment on the complementarity between the different techniques and their limitations. Whilst AFM imaging provide high resolution (1–5 nm) nanomorphology, the sampling area (~0.5–50 μm$^2$) is relatively small and localised. SANS probes a relatively much larger volume of the sample with a beam size of 7 × 10 mm and a sample thickness of 2 mm. The recorded scattering intensity is thus an average of that from a large number of aggregates of different sizes and geometries and the SANS analyses can yield structural information on the length scale of 5–100 nm (*cf.* Table 1). Cryo-TEM in this case provides an indication of the morphology with a limited resolution due to modest contrast and a very small sample size.

### LTA micellization in solution and the effect of $Ca^{2+}$ ions

The Cryo-TEM measurements provided information on the size and morphology of the formed aggregates at LTA concentration of 2 mg mL$^{-1}$ as shown in Fig. 2. The image suggests the formation of spherical structures with an average diameter of $D \sim 12 \pm 4.1$ nm in water (*cf.* Fig. 2A). The variations in the size distribution of LTA aggregates are shown in Fig. 2D. Due to its amphiphilicity, it is not surprising that LTA self-assembled into micelles at a concentration well about its reported CMC in aqueous solutions,[5,6] although the LTA micelle morphology has not been visualised previously.

**Table 1** Fitted SANS parameters for 2 mg mL$^{-1}$ LTA micelles as a function of $CaCl_2$ concentration [$CaCl_2$] at 25, 40 and 60 °C. Here $\xi_1$ and $\xi_2$ are the correlation lengths (in Å) corresponding to the low-$q$ (clusters) and high-$q$ (local structure) region of the SANS data curve, respectively. The $n$ (low-$q$) and m (high-$q$) values are the Lorentz exponents describing the LTA–water interactions, and $\chi^2$ an indication of the goodness of the fit

| [$CaCl_2$] (mM) | $\xi_1$ (Å) | $\xi_2$ (Å) | $n$ | $m$ | $\chi^2$ |
|---|---|---|---|---|---|
| **25 °C** | | | | | |
| 0 | 517 ± 14 | 16.8 ± 0.6 | 3.4 ± 0.02 | 4.2 ± 0.04 | 1.9 |
| 2 | 388 ± 12 | 34.7 ± 0.9 | 4.0 ± 0.07 | 2.6 ± 0.05 | 1.5 |
| 5 | 381 ± 14 | 33.9 ± 0.9 | 3.9 ± 0.08 | 2.7 ± 0.05 | 1.2 |
| 10 | 377 ± 13 | 33.1 ± 0.8 | 3.9 ± 0.07 | 2.8 ± 0.05 | 1.3 |
| **40 °C** | | | | | |
| 0 | 773 ± 35 | 17.9 ± 1.2 | 3.30 ± 0.02 | 3.1 ± 0.04 | 1.4 |
| 2 | 506 ± 27 | 32.0 ± 0.9 | 3.30 ± 0.07 | 2.7 ± 0.06 | 1.4 |
| 5 | 471 ± 28 | 32.4 ± 0.9 | 3.34 ± 0.08 | 2.8 ± 0.06 | 1.3 |
| 10 | 453 ± 22 | 31.5 ± 0.8 | 3.35 ± 0.07 | 3.0 ± 0.06 | 1.3 |
| **60 °C** | | | | | |
| 0 | 764 ± 25 | 19.7 ± 1.6 | 3.5 ± 0.03 | 2.7 ± 0.03 | 1.2 |
| 2 | 457 ± 19 | 32.8 ± 0.9 | 3.5 ± 0.07 | 2.7 ± 0.07 | 1.5 |
| 5 | 453 ± 21 | 30.3 ± 0.7 | 3.5 ± 0.07 | 3.1 ± 0.06 | 1.3 |
| 10 | 453 ± 21 | 30.0 ± 0.7 | 3.4 ± 0.06 | 3.2 ± 0.07 | 1.3 |

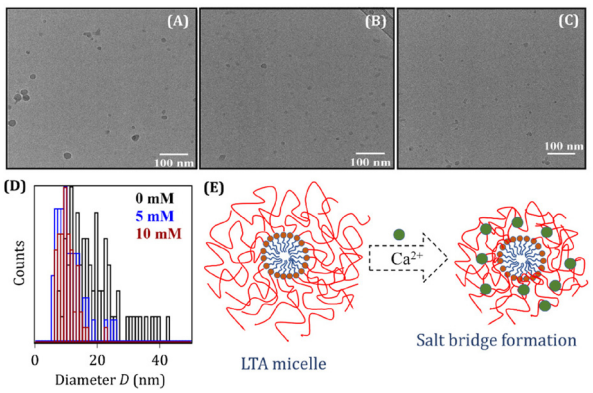


**Fig. 2** Cryo-TEM images of 2 mg mL$^{-1}$ aqueous LTA aggregates in (A) pure water, and in the presence of (B) 5 mM and (C) 10 mM $CaCl_2$. (D) The histogram showing variations in the size-distribution for the LTA aggregates. (E) Schematic representation of a spherical LTA micelle and changes caused by the addition of $CaCl_2$.

With addition of $CaCl_2$ (*cf.* Fig. 2B and C), a decrease in the size of aggregates to ~10 nm is evident presumably due to the electrostatic interactions between the negative charges of phosphate groups and $Ca^{2+}$ ions, leading to tighter packing of the chains in the shell region and the consequent shrinkage in the micelle size. The $Ca^{2+}$ ions can induce charge neutralisation by bridging the phosphate groups of neighbouring LTA chains.[24] The schematic in Fig. 2E illustrates the formation of LTA aggregates driven by the hydrophobic interactions among the hydrocarbon chains that formed the micelle core, while negatively charged hydrated polyglycerophosphate chains formed the shell. Earlier SAXS studies by Labischinski *et al.*[11] and Fischer *et al.*[12] also showed the formation of spherical micelles by LTA extracted from *Staphylococcus aureus* and

 

*Streptococcus pneumoniae*, both with an average diameter of ~23 nm but with the polymer chains adopting a highly coiled and a helical conformation, respectively, in the shell. Such structural assumptions about the coiled conformation of the polymer chain could be relevant to our study, considering the structural similarities in the LTA extracted from *Bacillus subtilis* and *Staphylococcus aureus*.

The microscopic evidence from the Cryo-TEM images in Fig. 2 on the formation of LTA micelles have not been reported previously. Pollack *et al.*[25] investigated the Benzylpenicillin assisted secretion of vesicles from the peripheral cell exterior of *Lactobacillus casei ATCC 7469* using Cryo-TEM. The results revealed vesicles formed by lipids and LTA mimicking the actual bacterial membrane compositions, although they formed distinct morphologies in the presence of different types of proteins. The balance between the electrostatic and steric forces between the LTA molecules and other membrane constituents, *e.g.* phospholipids and surface proteins, facilitates the formation of micelles or mixed vesicles. Our recent study[13] reported LTA induced structural changes in the mixed vesicles formed by LTA and phospholipids in a mixture representing their molecular composition in the *Bacillus subtilis* bacteria membrane. The LTA incorporation in the mixed vesicles up to 6.5 mol% concentration increased their size. As more LTA was added to the mixture, steric repulsion between LTA molecules favoured their partial partition from the mixed liposomes, forming LTA micelles in coexistence with the mixed liposomes.

### Nano-structural insights from small-angle neutron scattering (SANS) measurements

LTA aggregation behaviour in the presence of $CaCl_2$ was further investigated by SANS. Fig. 3 shows the variations in scattering intensities for 2 mg $mL^{-1}$ aqueous LTA solution in the presence of $CaCl_2$ at three different temperatures (25, 40, and 60 °C). The scattering intensity decreased with the addition of $CaCl_2$ up to 5 mM concentration and remains constant upon further increase to 10 mM (*cf.* Fig. S1(a) in ESI†). We attempted to fit this data using several models, *e.g.* the *gel fit*, the *Guinier Porod approximation*, the *correlation length model etc.* (*cf.* S1 in ESI†), but no physically relevant parameters could be achieved. Table 1 demonstrates fitted aggregation parameters using the two-Lorentzian model, which fits an empirical functional form to the SANS data characterised by two Lorentzian type functions. This model calculates two correlation lengths corresponding to the macro structure or clusters (low-$q$) and the local structure (high-$q$) as discussed below. With the presence of two main scattering regimes, it is conceivable that the high-$q$ regime corresponds to the LTA molecules and the LTA aggregates account for the scattering in the low-$q$ regime.

The Lorentzian exponents $n$ and $m$ (eqn (2)) are related to the extent of LTA–water interactions and an increase in these values account for unfavourable solvent–biopolymer interactions.[26] The calculated correlations lengths in the low-$q$ scattering data are much higher than the reported sizes of nascent LTA micelles,[11,12] which confirms the presence of clusters described by the correlation length ($\xi_1$). The gradual downturn (*cf.* Fig. S1(a) in ESI†) in the scattering intensity curve on increasing the $CaCl_2$ concentration (0–10 mM) indicates the decrease in the size of the formed clusters.

Fig. 4 plots the fitted correlation lengths ($\xi_1$ and $\xi_2$) as a function of $CaCl_2$ concentration at different temperatures. In the presence of 2 mM $CaCl_2$, the $\xi_1$ value decreased to 388 ± 12 Å from 517 ± 14 Å for LTA in water at 25 °C. Lorentzian exponent $n$ (low-$q$) increased to 4.0 ± 0.07 from 3.4 ± 0.02, indicating poorer LTA–water interaction on $CaCl_2$ addition, consistent with the formation of more compact and rigid structures

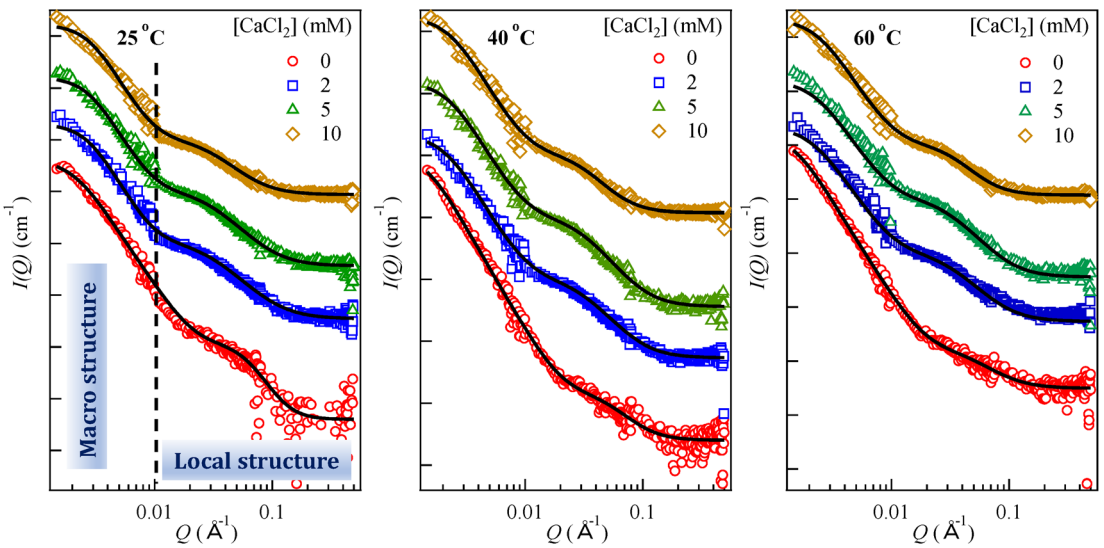


**Fig. 3** SANS intensity $I$ *vs.* $Q$ profiles for 2 mg $mL^{-1}$ LTA aqueous solutions containing 0–10 mM $CaCl_2$ at 25, 40 and 60 °C. Symbols are the data points and solid lines represent the best fits using the two Lorentzian model. For clarity, SANS profiles are scaled on the $y$-axis by a factor of 10, 100 and 1000, respectively, for the 2, 5 and 10 mM $CaCl_2$ data.

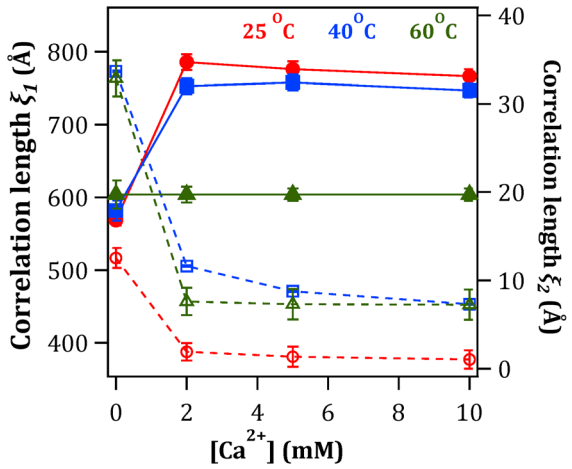


**Fig. 4** The fitted correlation lengths $\xi_1$ (low-$q$) and $\xi_2$ (high-$q$) in Å using the two-Lorentzian model for aqueous LTA aggregates in the presence of different $CaCl_2$ concentrations at different temperatures. The dash and solid lines are guides to the eye for $\xi_1$ and $\xi_2$ values, respectively.

due to the relatively long-lived salt-bridges between negatively charged phosphate centres of neighbouring LTA chains facilitated by $Ca^{2+}$ ions.[24] This high $n$ value thus suggests stronger inter-LTA interactions compared to those between water and LTA. These results support the Cryo-TEM data for pure LTA (*cf.* Fig. 2) depicting polydisperse large aggregates that decreased in the number density and size upon addition of $CaCl_2$. The $\xi_1$ and $n$ values are not sensitive to further increase in the $CaCl_2$ concentration to 5 mM and 10 mM.

A previous SANS analysis[27] on the aggregation of polyhedral oligomeric silsesquioxane dendrimers led to the interpretation of the presence of the structures with two length scales, attributed to global dendrimer aggregates and the intra-dendrimer local structure. In another report,[28] SANS characterization of globular polyprotein hydrogels revealed the presence of two length-scales with the scattering centres attributed to the regions of clustered polyproteins. The low-$q$ Lorentzian exponent values suggested surface fractals with a dimension in the range of 3 and 4, indicating rough surfaces of the scattering centres. Hammouda *et al.* also applied the correlation model[29] and the two-Lorentzian model[30] to their neutron scattering data from aqueous polyethyleneoxide (PEO) solutions to explain the clustering effect. Their results indicated an increase in the correlation length in the low-$q$ region with increasing PEO concentration due to PEO cluster growth, while the value in the high-$q$ region decreased, indicating shorter-range interactions. In another investigation, the microphase separation in the *N,N*-diethylacrylamide polymer hydrogels[31] after temperature-jump was analysed using the two-Lorentzian model that alluded to the presence of two phases: a dense phase corresponding to the equilibrium structure at the final temperature and a dilute nonequilibrium phase showing swollen a network after the temperature jump from 25 to 30 °C.

The average aggregate size obtained by Cryo-TEM (*cf.* Fig. 2D) may be compared with $\xi_1$. The correlation lengths ($\xi_1$ and $\xi_2$) are not the real size of aggregates but are indicative of the length scale of the spatial density/concentration fluctuations. For instance, for the semi-dilute polymer regime in hydrogels, the correlation length refers to the size of a "blob" or "mesh" of the polymer network. It may characterize the spatial correlation of concentration fluctuation in the system, *i.e.* the distance between entanglement points in the three-dimensional aggregate assemblies.[26] The calculated correlation length in the high-$q$ region ($\xi_2$) for pure LTA aggregates is 16.8 ± 0.6 Å, while the Lorentzian exponent $m$ is 4.2 ± 0.04. The former represents the dimension of a thermal blob originating from the fluid nature of the local concentration fluctuation in a semi-dilute polymer solution.[32] The fitted value for $\xi_2$ is much smaller than the molecular length of fully hydrated LTA molecule (~11 nm). Earlier SAXS investigations on aqueous aggregates of LTAs from *S aureus*[11] and *S. Pneumoniae*[12] calculated the radius of the spherical micelles ~11 nm (comparable to the size of fully extended LTA molecule), which indicates that the observed $\xi_2$ values are not correlated with the length of single LTA molecules. The structure of *B. subtilis* LTA studied here is similar to *S. aureus* LTA.[33] The small $\xi_2$ value arises from the intra-LTA local structure, instead of the free LTA molecules. With addition of 2 mM $CaCl_2$, the $m$ values decrease (4.2 ± 0.04 for 0 mM $CaCl_2$ to 2.6 ± 0.05). On the other hand, $\xi_2$ increased to 34.7 ± 0.9 Å from an initial value of 16.8 ± 0.6 Å in water, which indicates an expansion of the polymer. Thus, $\xi_2$ represents the short-range interactions involving LTA. Further increase of the concentration to 10 mM $CaCl_2$ led to only minor changes in the fitted parameters, suggesting relative insensitivity of the LTA local structure above 2 mM $CaCl_2$.

### Effect of temperature on LTA self-assembly

The SANS experiments were also performed at 40 and 60 °C. The higher temperature would promote the thermal motion and affect the solubility of the lipophilic chains in the LTA molecule and the mean molecular area.[13] With an increase in temperature, the scattering intensity in the low-$q$ region increased considerably, which indicates formation of large aggregates. In pure water, the fitted $\xi_1$ increased to 773 ± 34 Å at 40 °C from 517 ± 14 Å at 25 °C, and then decreased marginally at 60 °C. The corresponding $n$ value remained almost constant at ~3.4, indicating no further change in the LTA–water interactions up to 60 °C. The H-bonding formation could be disrupted at the higher temperature, which should result in reduced interactions between the polyglycerophopshate chains and water molecules. This should promote the hydrophobic interactions and favour the clustering of micelles. To counterbalance this, the increase in the temperature would also promote the fluidity of the LTA lipophilic chains, leading to a more open local structure of the polar chains. This is borne out in the trend of the increase in $\xi_1$ and decrease in $m$ with temperature in water (*i.e.* $\xi_1$ = 16.8 ± 0.6 Å, 17.9 ± 1.2 Å, and 19.7 ± 1.6 Å and $m$ = 4.2 ± 0.04, 3.1 ± 0.04, and 2.7 ± 0.03 at

25 °C, 40 °C, and 60 °C, respectively). The marginal decrease in the $\xi_1$ value at 60 °C could also be attributed to the delicate balance between dehydration and chain fluidization, which led to more compact packing of the micelles due to dehydration of polar chains and the overall slightly smaller cluster size compared to 40 °C.

However, the trends of the $\xi_2$, $n$ and $m$ values with the temperature are not clear-cut in the presence of different $CaCl_2$ concentrations of 2, 5 and 10 mM (*cf.* Table 1). Nonetheless, the decrease in $\xi_1$ with temperature under all the $CaCl_2$ concentrations indicates more compact cluster size, attributed to neutralisation and bridging of LTA phosphates by $Ca^{2+}$. The $\xi_2$ values at 40 and 60 °C were also consistently larger compared to those at 25 °C under all the $CaCl_2$ concentrations, indicative of a more open network structure due to enhanced chain fluidity, whilst the increasing $Ca^{2+}$ concentration again caused $\xi_2$ to decrease slightly at all the temperatures. Similarly, the low-$q$ Lorentzian exponent $n$ values were consistently smaller at 40 °C and 60 °C as compared to 25 °C, which is particularly pronounced in the presence of $Ca^{2+}$; whilst the high-$q$ Lorentzian exponent $m$ value remained slightly changed (2.6–3.2) at all temperatures in the presence of $Ca^{2+}$, with the exception of $m \sim 4.2$ in pure water at 25 °C indicating poorer water–LTA interactions. These structural changes in response to temperature and $Ca^{2+}$, as revealed by SANS, point to the intricate interplays between hydration and chain flexibility which are made more complex by temperature and divalent cations.

### Interfacial adsorption behaviour of LTA aggregates

Control AFM measurement using 2 mg $mL^{-1}$ LTA aggregates indicated little adsorption at the mica–water interface (featureless images not shown), which may be attributed to the highly negatively charged mica surface repelling similar charged LTA,[34,35] pointing to the importance of the electric double layer interactions in LTA surface adsorption. With the addition of 10 mM $CaCl_2$, the adsorption of the LTA aggregates on the mica surface increased due to neutralisation and likely overcompensation of the negative LTA charges by $Ca^{2+}$ (*cf.* Fig. S2(a) and S2(b) in ESI†). Redeker and Briscoe[15] similarly reported enhanced adsorption of negatively charged lipopolysaccharides (LPS) on mica in the presence of $Ca^{2+}$, which was attributed to the bridging effect between LPS molecules and between LPS and mica.

Further AFM imaging was attempted on the $SiO_2$ substrate in the presence of $CaCl_2$ to correlate with the QCM-D results. To compare the effect of lower LTA concentration and establish a correlation with the QCM-D experiments (discussed later, *cf.* Fig. 7), AFM images of 0.2 mg $mL^{-1}$ LTA aggregates adsorbed on $SiO_2$ substrates are shown in Fig. 5. In pure water, limited adsorption of LTA aggregates was observed (Fig. 5A and B) at 25 and 40 °C, and the LTA aggregates also appeared to be easily removed by the scanning AFM tip during the measurements, indicating weak adsorption at the interface due to strong repulsion minimising the contacts between the negatively charged LTA glycerophosphate chains and the $SiO_2$ surface. At 40 °C, the presence of a few large aggregates is evident, confirming the temperature assisted clustering as observed at higher LTA concentrations.

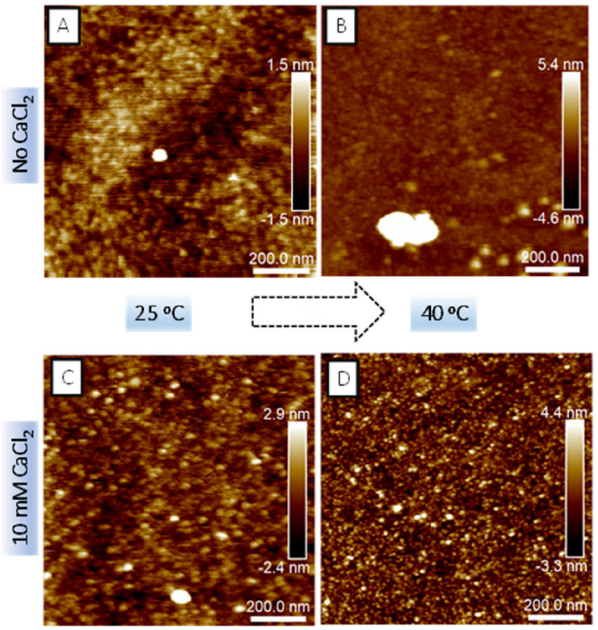


**Fig. 5** AFM images showing the topography of 0.2 mg $mL^{-1}$ LTA aggregates adsorbed at the $SiO_2$–water interface in pure water at (A) 25 °C; (B) 40 °C, and 10 mM $CaCl_2$ at (C) 25 °C; (D) 40 °C.

Due to the limited resolution of these images, the lateral sizes could not be estimated precisely. The LTA aggregates shown in Fig. 5(B) indicated the presence of two size distributions around 8–10 nm and ~30 nm. As shown in Fig. 5C and D, the addition of 10 mM $CaCl_2$ greatly promoted LTA aggregate adsorption, with spherical structures evident on the surface. At 25 °C, the calculated average size of these structures was 29.6 ± 5.2 nm. Interestingly, the average size decreased to 16.0 ± 2.1 nm at 40 °C indicating shrinking of the aggregates.

Fig. 6 shows the topography of 2 mg $mL^{-1}$ LTA aqueous aggregates in the presence of 10 mM $CaCl_2$ at the $SiO_2$–water interface at 25 °C (Fig. 6A–C) and 40 °C (Fig. 6D–F). The calculated $Z$-axis height $h$ of these adsorbed structures at the $SiO_2$–water interface was 6.5 nm at 25 °C, which increased to 9.2 nm at 40 °C. Fig. 6A reveals a dense coverage by spherical LTA aggregates within the scan area of 5 μm × 5 μm at 25 °C. On increasing the incubation temperature to 40 °C, the surface coverage by the LTA aggregates increased and further adsorbed layers of the spherical structures developed (*cf.* Fig. 6D). The calculated lateral diameter of the spherical LTA aggregates increased from 46 ± 10 nm at 25 °C to 77 ± 20 nm at 40 °C. These values were considerably higher than those obtained by the Cryo-TEM measurements (*cf.* Fig. 2). Thus, the large aggregates adsorbed at the interface were attributed to clustering of LTA micelles consistent with the SANS analysis. Higher resolution scans (*cf.* Fig. 6B and C) further revealed the "*raspberry*" structure of the surface aggregates, showing clusters by 3–6

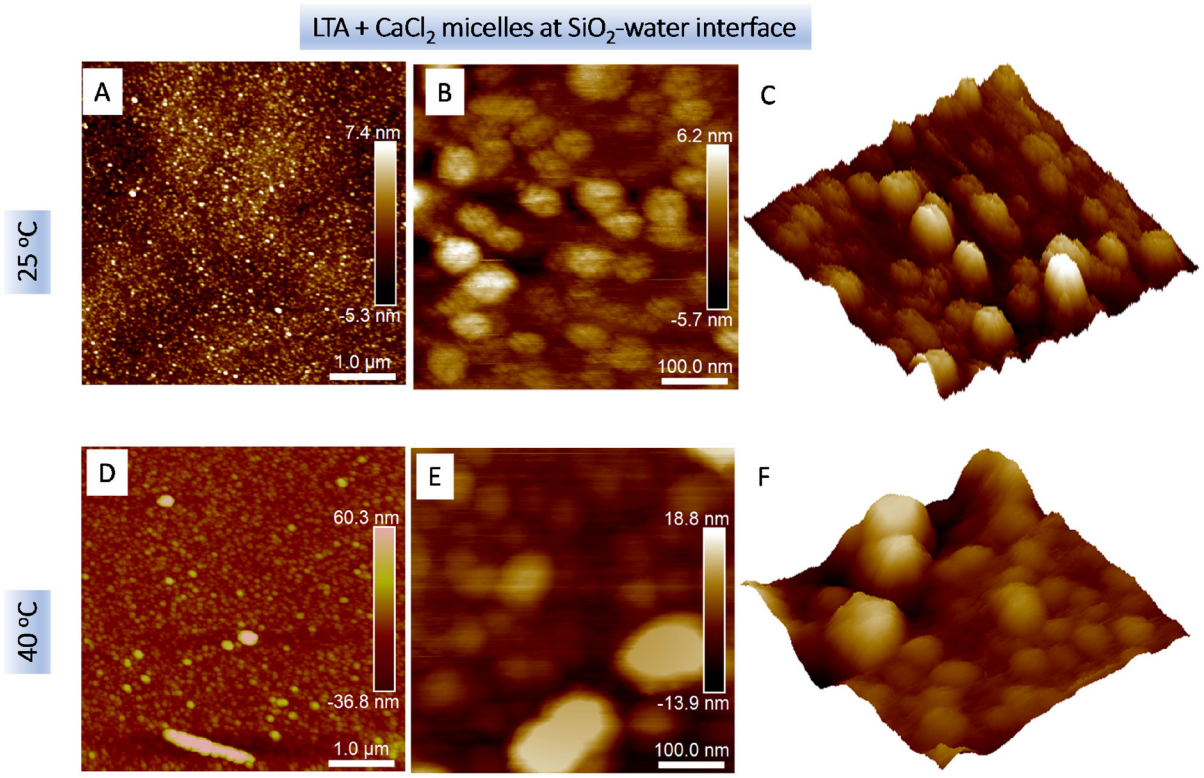


**Fig. 6** AFM images for 2 mg $mL^{-1}$ LTA aggregates in the presence of 10 mM $CaCl_2$ adsorbed on $SiO_2$–water interface at different incubation temperatures. (A, B and C) 25 °C; (D, E and F) 40 °C. The scan size for A and D is 5 μm × 5 μm, whist that for B and E 500 nm × 500 nm. C and F show the 3D image for B and E, with the same height scale, respectively.

nascent LTA micelles, thus, pointing to ~10–$10^2$ micelles per cluster, presumably formed due to stronger inter-aggregate interactions due to a combination of inter-micelle H-bonding and $Ca^{2+}$ bridging. Fig. S2(c) in the ESI section† shows the raspberry structure observed from three different sizes. AFM imaging at 40 °C (*cf.* Fig. S2(d) and (e)†) showed the presence of elongated structures and the presence of larger spherical structures, which indicated inhomogeneous clustering of micelles due to a decrease in the hydration around LTA aggregates and an increased chain fluidity of the hydrocarbon chain that results in larger area occupied by the LTA molecules. The 2 mg $mL^{-1}$ LTA solution contained a large number of LTA micelles existing at smaller inter-micellar distances. By comparison, at 0.2 mg $mL^{-1}$ LTA concentration, aggregates were less susceptible to clustering due to considerably lower micellar density and larger inter micellar distances.

These results are broadly in agreement with the SANS data that showed an increase in the size of the LTA aggregates on increasing the temperature to 40 °C. Fig. 6E shows an example of the presence of a considerably larger non-spherical aggregate (*cf.* also Fig. S2(d) and (e)†). Fig. 6F shows the presence of clusters although the individual LTA micelles constituting the clusters were not resolved, possibly due to enhanced fluidity of the micelle–water interface at the elevated temperature. These observations are consistent with the SANS analysis indicating the presence of two correlation lengths describing the presence of clusters in the low-$q$ region.

### QCM-D investigations on LTA aggregates adsorbed on $SiO_2$ substrate

Fig. 7 shows the resonant frequency shift $\Delta f$ and the dissipation shift $\Delta D$ as a function of deposition time of 0.2 mg $mL^{-1}$ LTA in Milli-Q water and in 10 mM $CaCl_2$ aqueous solution. The frequency change $\Delta f$ (*cf.* Fig. 7A) reflects the amount of LTA adhering to the $SiO_2$ surface, and the dissipation $\Delta D$ (*cf.* Fig. 7B) informs on the morphology of the adsorbed layer. In pure water, the $\Delta f$ and $\Delta D$ values changed only slightly, suggesting negligible adsorption, consistent with the AFM observations above. Upon rinsing with 10 mM $CaCl_2$, a decrease in $\Delta f$ and an increase in $\Delta D$ was observed due to the adsorption of divalent $Ca^{2+}$ ions on the negatively charged $SiO_2$ crystals sites. Furthermore, it is evident that the addition of 10 mM $CaCl_2$ imparted a significant effect on the adsorption behaviour of LTA aggregates. The frequency decreased initially as a result of LTA adsorption, and then increased towards a plateau value, indicative of LTA desorption upon rinsing with the pure water. By applying the Voigt viscoelastic model, the final mass ($m_{fin}$) and the final thickness ($t_{fin}$) were determined. The final frequency change ($\Delta f_{fin}$ = −24.0 Hz) corresponds to an adsorbed $m_{fin}$ of 420.9 ng $cm^{-2}$ and the $t_{fin}$

 

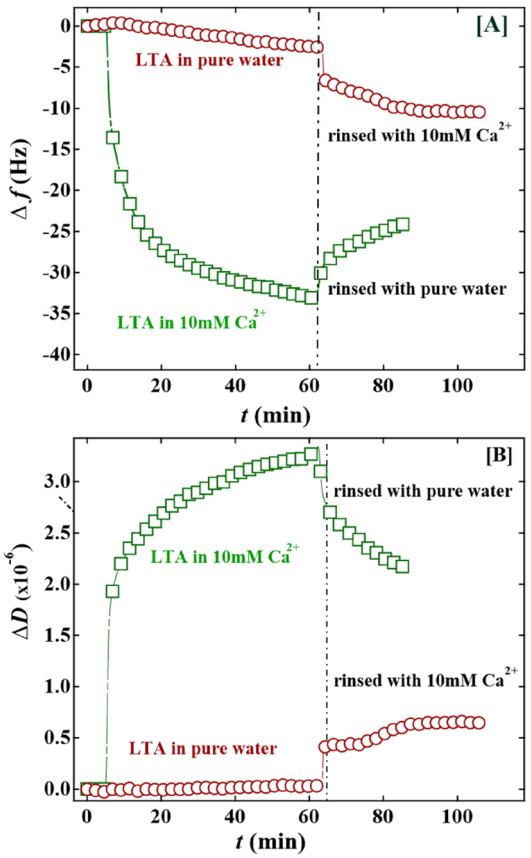


Fig. 7 Variations in the resonant frequency ($\Delta f$) and dissipation shifts ($\Delta D$) as a function of deposition time ($t$) for 0.2 mg mL$^{-1}$ LTA aqueous solution in pure water (A) and in the presence of 10 mM $CaCl_2$ (B) at 25 °C. The time dependence of frequency shift and dissipation is given for the 7$^{th}$ overtone.

of the adsorbed LTA layer was estimated to be 3.2 nm assuming the adsorbed LTA layers had a density of 1.3 g cm$^{-3}$. These results are in good agreement with the AFM images (*cf.* Fig. 6), indicating $Ca^{2+}$ promoted the adsorption of the LTA aggregates at the $SiO_2$–water interface. The estimated layer thickness ~3.2 nm points to deformed or compacted LTA aggregates due to the shrinking of the polar chains caused by the salt-bridge formation that also facilitates the adsorption at the charged $SiO_2$ surface. It is conceivable that LTA adsorbed as isolated clusters rather than a homogenous film, which would affect the accuracy of QCM analyses. Nonetheless, the QCM results concurred with the AFM imaging that the $Ca^{2+}$ addition promoted LTA adsorption on the negatively charged $SiO_2$ surface.

## Conclusions

Self-assembly and adsorption behaviour of lipoteichoic acid (LTA), a polymeric amphiphile extracted from *Bacillus subtilis*, has been investigated in the presence of $CaCl_2$ (2, 5 and 10 mM) and at different temperatures (25, 40, and 60 °C). The nanostructures from self-assembly and hierarchical clustering of the simple model LTA systems on different length scales are complex. There is not a single definitive technique that could probe unequivocally the structures on all length scales. This serves to demonstrate the value in undertaking fundamental studies of LTA self-assembly using complementary physicochemical methods. The Cryo-TEM images revealed formation of spherical micelles ($D \sim 12$ nm) that decreased in size upon addition of $CaCl_2$. The electrostatic charge neutralisation at the phosphate-decorated surface of LTA micelles and the formation of inter-LTA salt-bridges resulted in the shrinking of the micelle shell. The analysis of the SANS data using the two-Lorentzian model indicated the presence of two correlation lengths for, respectively, the clusters ($\xi_1$, low-$q$) and the local structures due to intra- and inter-LTA correlations ($\xi_2$, high-$q$). These two correlations gave insights into the LTA aggregate structure which depended sensitively on the interplays of the polyglycerophosphate chain flexibility and hydration (or H-bonding) capacity, both affected by both temperature and the presence of divalent $Ca^{2+}$. The decrease in $\xi_1$ on the addition of $CaCl_2$ can be attributed to the formation of stable and long-lived salt-bridges between the negatively charged phosphate groups (both intra- and inter-chain). The corresponding increase in the Lorentzian exponent $n$ (low-$q$) points to the decreased interactions between water and LTA. On the other hand, the $\xi_2$ values increased with $Ca^{2+}$ addition, which indicates an increase in the intra-LTA correlations. With an increase in the temperature, the LTA clusters grew in size due to the enhanced hydrophobic interactions from dehydration between nascent LTA micelles, possibly overcompensating for the steric interactions arising from enhanced LTA chain fluidity. Our results on the effect of the $Ca^{2+}$ addition suggest that the hydrated polyglycerophopshate chains likely adopt a relatively extended conformation in the LTA micellar shell in water. Loose aggregates may form due to interpenetration of the chains between neighbouring micelles. With the addition of $Ca^{2+}$, the resultant neutralization or bridging leads to more compact micellar structures.

AFM imaging revealed an increase in the surface LTA coverage at the $SiO_2$–water interface at 40 °C and particularly in the presence of $Ca^{2+}$ which acts to bridge the negatively charged LTA and $SiO_2$. The LTA adsorption coverage and morphology depended on the concentration of both LTA and $Ca^{2+}$. In 2 mg mL$^{-1}$ LTA, further adsorption of the LTA aggregates atop the underlying layer was evident and the raspberry-like clusters with ~10–100 LTA micelles were also observed in 10 mM $Ca^{2+}$ at 25 °C. The QCM-D results were consistent with the AFM results, showing a decrease in the resonant frequency $\Delta f$ and an increase in the dissipation $\Delta D$ in the presence of 10 mM $CaCl_2$, which indicates a significant adsorption at the $SiO_2$–water interface. These unprecedented results point to the intricate and complex interplays between LTA and water molecules, sensitively dependent on divalent cations and solution temperature, that underpin self-assembly of *Bacillus subtilis* LTA in solution and at the solid–water interface. Such fundamental insights are relevant to our understanding of LTA-mediated bacterial adhesion, colonisation, and sepsis. In a further publi-

cation, we will discuss how the structure of the LTA monolayer at the air–water interface can be affected by the presence of mono-/di-/tri-valent cations at different temperatures.

## Conflicts of interest

There are no conflicts to declare.

## Acknowledgements

We acknowledge the Institut Laue-Langevin (ILL) for the awarded beamtime under experiment number: 9-13-912 [https://doi.ill.fr/10.5291/ILL-DATA.9-13-912]. We thank Lauren Matthews and Xueying Guo for their help with the SANS measurements and useful discussions. We also acknowledge the Wolfson Foundation for establishing the Wolfson Bioimaging Facility, University of Bristol. This project has received funding from the European Union's Horizon 2020 Research and Innovation Programme under the Marie Skłodowska-Curie grant agreement SoftNanoHybrid no. 797038 (Bhavesh Bharatiya) and grant agreement HYDRA no. 793574 (Gang Wang). WHB would like to acknowledge funding from Engineering and Physical Science Research Council (EPSRC; EP/H034862/1 and EP/H014861/1). MW and PW acknowledge support from the Ministerstwo Edukacji i Nauki *via* the statutory subsidy for Jerzy Haber Institute of Catalysis and Surface Chemistry PAS.

## References

1 I. Ginsburg, *Lancet Infect. Dis.*, 2002, **2**(3), 171–179.
2 I. Fedtke, D. Mader, T. Kohler, H. Moll, G. Nicholson, R. Biswas, K. Henseler, F. Götz, U. Zähringer and A. Peschel, *Mol. Microbiol.*, 2007, **65**(4), 1078–1091.
3 M. Gross, S. E. Cramton, F. Götz and A. Peschel, *Infect. Immun.*, 2001, **69**(5), 3423–3426.
4 C. Weidenmaier, J. F. Kokai-Kun, S. A. Kristian, T. Chanturiya, H. Kalbacher, M. Gross, G. Nicholson, B. Neumeister, J. J. Mond and A. Peschel, *Nat. Med.*, 2004, **10**(3), 243–245.
5 A. J. Wicken, J. D. Evans and K. W. Knox, *J. Bacteriol.*, 1986, **166**(1), 72–77.
6 H. S. Courtney, W. A. Simpson and E. H. Beachey, *Infect. Immun.*, 1986, **51**(2), 414–418.
7 A. Helenius and K. Simons, *Biochim. Biophys. Acta, Biomembr.*, 1975, **415**(1), 29–79.
8 C. Tanford, *Science*, 1978, **200**(4345), 1012–1018.
9 J. L. Markham, K. W. Knox, A. J. Wicken and M. Hewett, *Infect. Immun.*, 1975, **12**(2), 378–386.
10 P. Harrop, R. O'Grady, K. W. Knox and A. J. Wicken, *J. Periodontal Res.*, 1980, **15**(5), 492–501.
11 H. Labischinski, D. Naumann and W. Fischer, *Eur. J. Biochem.*, 1991, **202**(3), 1269–1274.
12 W. Fischer, S. Markwitz and H. Labischinski, *Eur. J. Biochem.*, 1997, **244**(3), 913–917.
13 B. Bharatiya, G. Wang, S. E. Rogers, J. S. Pedersen, S. Mann and W. H. Briscoe, *Colloids Surf., B*, 2021, **199**, 111551.
14 A. Tripathy, P. Sen, B. Su and W. H. Briscoe, *Adv. Colloid Interface Sci.*, 2017, **248**, 85–104.
15 C. Redeker and W. H. Briscoe, *Langmuir*, 2019, **35**(48), 15739–15750.
16 G. Sauerbrey, *Z. Phys.*, 1959, **155**(2), 206–222.
17 F. Höök, M. Rodahl, P. Brzezinski and B. Kasemo, *Langmuir*, 1998, **14**(4), 729–734.
18 M. Rodahl, F. Höök, A. Krozer, P. Brzezinski and B. Kasemo, *Rev. Sci. Instrum.*, 1995, **66**(7), 3924–3930.
19 M. V. Voinova, M. Rodahl, M. Jonson and B. Kasemo, *Phys. Scr.*, 1999, **59**(5), 391.
20 K. Lieutenant, P. Lindner and R. Gahler, *J. Appl. Crystallogr.*, 2007, **40**(6), 1056–1063.
21 https://www.ill.eu/users/instruments/instruments-list/d11/description/instrument-layout.
22 B. Bharatiya, G. Wang and W. H. Briscoe, *et al.*, *Mixed liposomes containing bacterial lipoteichoic acid (LTA)*, Institut Laue-Langevin (ILL), 2020, DOI: 10.5291/ill-data.9-13-912.
23 https://www.sasview.org/docs/user/models/two_lorentzian.html.
24 M. Sammalkorpi, M. Karttunen and M. Haataja, *J. Phys. Chem. B*, 2009, **113**(17), 5863–5870.
25 J. H. Pollack, A. S. Ntamere and F. C. Neuhaus, *Microbiology*, 1992, **138**(5), 849–859.
26 F. Horkay and B. Hammouda, *Colloid Polym. Sci.*, 2008, **286**(6), 611–620.
27 G. Yuan, X. Wang, D. Wu and B. Hammouda, *Polymer*, 2016, **100**, 119–125.
28 M. A. Da Silva, S. Lenton, M. Hughes, D. J. Brockwell and L. Dougan, *Biomacromolecules*, 2017, **18**(2), 636–646.
29 B. Hammouda, D. L. Ho and S. Kline, *Macromolecules*, 2004, **37**(18), 6932–6937.
30 B. Hammouda, D. Ho and S. Kline, *Macromolecules*, 2002, **35**(22), 8578–8585.
31 J. Pleštil, M. Ilavský, H. Pospíšil, D. Hlavatá, Y. M. Ostanevich, G. Degovics, M. Kriechbaum and P. Laggner, *Polymer*, 1993, **34**(23), 4846–4851.
32 K. J. Lee and S. I. Yun, *Polymer*, 2018, **139**, 86–97.
33 N. T. Reichmann and A. Gründling, *FEMS Microbiol. Lett.*, 2011, **319**(2), 97–105.
34 J. N. Israelachvili and G. E. Adams, *J. Chem. Soc., Faraday Trans.*, 1978, **74**, 975–1001.
35 J. N. Israelachvili, *Intermolecular and surface forces*, Academic Press, London, 2nd edn, 1992.